AIAA 95-0525

Velocity Measurements for a Sonic Underexpanded Transverse Jet Injected Into a Supersonic Flow

J.G. Santiago and J.C. Dutton
Department of Mechanical and Industrial Engineering
University of Illinois at Urbana-Champaign
Urbana, Illinois 61801

33rd Aerospace Sciences Meeting and Exhibit
January 9-12, 1995 / Reno, NV

VELOCITY MEASUREMENTS FOR A SONIC UNDEREXPANDED TRANSVERSE JET INJECTED INTO A SUPERSONIC FLOW

J.G. Santiago* and J.C. Dutton†
Department of Mechanical and Industrial Engineering
University of Illinois at Urbana-Champaign
Urbana, Illinois 61801

Abstract

Transverse jet injection into a supersonic flow (TJISF) is a promising method of achieving the injection, mixing, and combustion of fuel in new supersonic combustion engines. The present investigation uses measurements of the mean and fluctuating components of the TJISF velocity field to study fluid dynamic mechanisms and mixing processes. The study provides velocity measurements using a two-component, frequency pre-shifted LDV system together with an automatic traverse system. Over 2,200 measurement locations are concentrated in the transverse, midline plane. These measurements help resolve issues such as the size and orientation of the recirculation regions upstream and downstream of the jet, the velocity of the jet in the barrel shock structure, the Mach number immediately preceding the Mach disk, the Reynolds stresses of the mixing layers, and the overall structure of the mean flow and turbulence fields.

Nomenclature

C_f = skin friction coefficient
d = jet diameter
H = compressible shape factor, δ^*/θ
M = Mach number
P = pressure
U = mean streamwise velocity
u' = fluctuating component of streamwise velocity
u_τ = friction velocity
V = mean transverse velocity
v' = fluctuating component of transverse velocity
x = streamwise coordinate
y = transverse coordinate
z = spanwise coordinate
γ = specific heat ratio
δ = boundary-layer thickness
δ^* = displacement thickness
θ = momentum thickness
ν_w = kinematic viscosity at wall
Π = wake strength parameter
ρ = density
$\langle\rangle$ = ensemble-averaged value

Subscripts
j = condition at jet nozzle exit
c = crossflow condition

Superscripts
$()'$ = fluctuating value

*Graduate Research Assistant, Student Member AIAA.
†Professor, Associate Fellow AIAA.

Introduction

Resurgent interest in the development of supersonic combustors has motivated the study of transverse jet injection into a supersonic flow (TJISF). The need to inject, mix, and burn fuel quickly and efficiently is important because of the short residence times associated with supersonic combustors. The design of a supersonic combustor which uses TJISF as a means of fuel injection and mixing requires a fundamental understanding of these flows.

The present investigation is a quantitative, experimental study of a single, sonic, underexpanded TJISF. The motivation for this study is to improve the understanding of the fluid dynamic mechanisms and mixing processes in this flow. In addition, the study provides benchmark data that may be used for the analytical and numerical modeling of these flows. To this end, schlieren/shadowgraph photography and two-component laser Doppler velocimetry (LDV) data have been obtained. This paper presents a discussion of the qualitative structure of the TJISF flowfield, a short review of the pertinent literature, a description of the experimental facility and the diagnostic techniques used, and a presentation and discussion of the velocity measurements obtained in the transverse, midline plane.

Flowfield Structure

A schematic of a typical underexpanded TJISF flowfield is shown in Fig. 1. The plane shown in this figure is hereafter referred to as the midline, transverse plane of this flowfield. The figure shows the supersonic freestream flowing from left to right with the jet injected through the bottom wall. The obstruction caused by the jet generates a bow shock in the freestream. A small recirculation region near the

surface is created just ahead of the jet. The internal structure of the jet itself is similar to that of a gaseous jet injected into a quiescent medium[1]. After leaving the orifice, the high pressure, underexpanded jet expands through a Prandtl-Meyer fan centered at the nozzle lip before compressing through an interception shock structure (i.e., a barrel shock) and a Mach disk. As it passes through the Mach disk, the jet fluid loses much of its momentum and is then quickly turned downstream. Much of the jet fluid, however, passes through the oblique shocks which define the sides of the barrel shock. Downstream of the barrel shock structure, the jet cross section grows as it is further mixed into the crossflow. Immediately downstream of the jet and near the surface is another recirculation region.

Background

There have been numerous studies of the fluid mechanics of the TJISF flowfield. The impetus for such research has been the study of supersonic combustor fuel injection, thrust vector control of rocket nozzles, and jet reaction force prediction. As a result of these studies, the qualitative structure of the TJISF flowfield is fairly well understood. In addition, there have been a number of quantitative studies concerning the description of the TJISF flowfield structure and mixing characteristics.

An early analytical model by Schetz and Billig[2] predicts the jet trajectory downstream of the Mach disk by balancing inertial, pressure, and drag forces along the jet arc. The authors compare the results of this drag model with experimental data. The model predicts the jet trajectory fairly well for jet-to-crossflow momentum flux ratios of about five. The location of the Mach disk (and, hence, the origin of the calculated trajectory) is determined by drawing on the analogy between the TJISF and free jet flowfields. Namely, the free jet model of Adamson and Nicholls[1] is used to estimate the Mach disk height given an estimate of the "effective back pressure." This effective back pressure, P_{eb}, is viewed as the pressure which determines the degree of expansion of the jet and is a function of the complex pressure field in the region near the exit of the jet. This idea of an effective back pressure has become a standard concept in the discussion of the fluid dynamics of the TJISF flowfield. Also, these authors identified the jet-to-crossflow momentum flux ratio as the most important parameter that determines jet penetration. This ratio, J, may be written as

$$J \equiv \frac{\rho_j V_j^2}{\rho_c V_c^2} = \frac{\gamma_j P_j M_j^2}{\gamma_c P_c M_c^2} \qquad (1)$$

where ρ, V, γ, P, and M are density, velocity, specific heat ratio, pressure, and Mach number, respectively; the subscripts j and c indicate properties of the jet and crossflow.

Billig et al.[3] present a discussion of many of the mathematical and physical concepts used in the study of the penetration characteristics of TJISF. Included is a detailed discussion of the analogy between the free jet and TJISF flowfields and a discussion of the idea of the effective back pressure. These authors developed an analytical model which predicts jet trajectory, location of the Mach disk, and the jet cross-sectional area as a function of the trajectory location.

Heister and Karagozian[4] present a model which predicts the trajectory and mixing characteristics of TJISF. The jet cross-section is modeled as a counter-rotating, compressible vortex pair. This is consistent with the vortex pairs observed in experiments which visualize the cross-sections of TJISF. The interaction of this vortex pair with the freestream is achieved by developing mass and momentum balances along the axis of the jet. A numerical technique is used to solve for the inviscid outer flow and to predict the geometry of the leading bow shock. The solution does not incorporate a model of the Mach disk and is, therefore, only valid for perfectly expanded or slightly underexpanded jets.

There have been several three-dimensional numerical studies of circular jets injected into supersonic flows[5-8]. All of the studies referred to here have solved the three-dimensional, compressible, Reynolds-averaged, Navier-Stokes equations using the Baldwin-Lomax turbulence model. Many of these studies show good comparison with experimental data. However, the results of these numerical studies were compared with only jet wall pressure and jet penetration data. Comparison with jet penetration does not ensure that a code correctly models jet spreading, jet mixing, turbulent kinetic energy production, or many other aspects of the velocity field. Also, Segal et al.[6] show that comparison with jet wall pressure data is not an adequate validation of a numerical solution. Riggins and McClinton[9] show that their numerical predictions agree well with both jet wall pressure and molecular concentration data. However, like the studies above, there are no quantitative comparisons with velocity field data.

There have been numerous experimental studies of jets injected into crossflows. Several studies have obtained quantitative measurements of the velocity fields of jets injected into *subsonic* crossflows[10-13]. All of the experimental studies discussed here have used hot wire anemometry to measure the mean and

fluctuating velocity fields. A notable study is that of Andreopoulos and Rodi[13] who used three-sensor hot wire anemometry to obtain three component mean velocity measurements and all six Reynolds stresses. These researchers present a discussion of the turbulent shear stresses throughout the subsonic, transverse jet flowfield and of the development of turbulent kinetic energy in this flow. Measurements were taken in the transverse plane at both the midline and at the off-midline location of z/d = 0.5 (see Fig. 1 for a definition of the coordinate system). Also, discussions are presented of the expected vorticity field in the near-jet region and of the kidney-shaped pair of counter-rotating vortices observed in the crossflow planes of the jet.

Several experimental studies have also determined various aspects of the structure of jets injected into a *supersonic* flow. These descriptions of the structure include shock shape and location, jet concentration profiles throughout the flowfield, the geometry of the separation regions upstream and downstream of the jet, and the static pressure field near the jet orifice. Zukoski and Spaid[14] described many of the features of the flowfield using schlieren and shadowgraph photography, static pressure measurements at the jet wall (using pressure taps), and concentration measurements in the flow. Schetz et al.[15] used schlieren and shadowgraph photography to further describe the qualitative flow structure of the transverse jet itself. These authors established the very useful analogy between the TJISF flowfield and the flowfield of an underexpanded jet injected into a quiescent medium (i.e., a free jet). A detailed description of the jet interception shock and Mach disk is presented. Other studies of jet penetration include those of Schetz et al.[16] and Cohen et al.[17]

Recent studies have provided further descriptions of the structure of the TJISF flowfield using laser-based flow visualization measurement techniques[18-22]. These studies used laser-induced fluorescence (LIF) and Mie scattering to study jet mixing and to visualize large-scale turbulent structures. The study of VanLerberghe et al.[22] was performed in the same experimental facility and presents a comparison of multiple planar laser-induced fluorescence (PLIF) images of TJISF at the same flow conditions as the present study. When such images are superimposed, they show that the bow shock generated by the obstruction of the jet is steady (at least in this facility). However, superimposed images of the barrel shock suggest that this flow structure contains regions of unsteadiness. The most apparent unsteady region is on the windward side of the barrel shock. This region of the barrel shock appears to be slightly flattened in some of the images.

Papamoschou et al.[23] performed an experimental parametric study of TJISF penetration versus relevant flow parameters. As expected, they found that jet penetration depends mainly on the jet-to-crossflow momentum flux ratio. Jet penetration is only a weak function of the jet-to-crossflow Mach number ratio. Although the correct value of effective back pressure for a transverse jet in supersonic crossflow is not well understood, Papamoschou et al.[23] suggested an effective back pressure equal to 30% of the static pressure behind the normal portion of the bow shock. Also, these authors showed that jet penetration seems to be maximized at the condition where the static pressure at the jet exit matches the effective back pressure. The difference in penetration between "pressure-matched" and underexpanded jets, however, is small.

There are a few studies which provide either quantitative or semi-quantitative measurements of the velocity fields of underexpanded jets injected into a supersonic flow[24-28]. These studies used either pointwise LIF or PLIF to make velocity, temperature, pressure, and concentration measurements. However, the velocity measurements of these studies are limited to time-averaged measurements of mean velocities and are not as accurate as the present LDV study. Two of these studies[27,28] also employed LDV to measure mean and fluctuating velocity components. However, these LDV measurements were used primarily to compare selected profiles to those of the PLIF measurements and not to map out the mean velocity and turbulence fields. In both cases, only five LDV velocity profiles in the midline, transverse plane were reported.

To date, only one previous study is known which uses LDV as the primary diagnostic in the study of the mean and fluctuating velocity field of TJISF. This work has been performed by Gallard et al.[29] at ONERA in Chatillon, France. These workers investigated the effect of jet heating on jet spreading in the TJISF flowfield using three-component LDV measurements, Pitot probe measurements, and temperature measurements using thermocouples. Although this AGARD publication is written in French, a preliminary translation of this report indicates that these authors studied the effects of temperature on jet spreading and on the mean and turbulent velocity fields. The measurements presented were obtained in four crossflow planes (i.e., planes in the spanwise and transverse directions).

Despite the numerous investigations discussed above, it is clear that a dearth of non-intrusive, quantitative measurements exists for the velocity field

in the TJISF flowfield. Such measurements will add to the fundamental understanding of the fluid dynamic mechanisms and mixing processes of this flow. The current investigation uses LDV measurements of the mean and turbulent velocity fields in order to study the characteristics of a sonic, underexpanded transverse jet injected into a Mach 1.6 crossflow. The experiments described in this paper provide two mean velocity components U and V as well as three of the six Reynolds stresses $\langle u'^2 \rangle$, $\langle v'^2 \rangle$, and $\langle u'v' \rangle$ (Fig. 1). These measurements are taken in the x-y, midline plane.

Experimental Facility

The experiments performed in this study use the air delivery system of the Gas Dynamics Laboratory. This facility has two compressors arranged in parallel which provide a 115 m^3 tank farm with about 1 kg/s of air at 862 kPa. A 4 inch Valtek control valve installed on the output side of the tank farm is used to control wind tunnel plenum pressure. A Fisher TL101 Process Controller is used to provide the 4-20 mA signal needed to actuate the upstream control valve. A 0-690 kPag Setra pressure sensor installed in the wind tunnel plenum provides the controller with a 0-5 V pressure signal as feedback. The feedback system provides a constant wind tunnel plenum pressure during blowdown of the tank farm. Finally, an Omega type K thermocouple in the plenum chamber is used to measure the wind tunnel air stagnation temperature.

The supersonic wind tunnel has a Mach 1.6 nozzle and is 76 mm wide over the entire length. The wind tunnel test section is 36 mm high. Flow conditioning is accomplished just upstream of the wind tunnel nozzle by means of a short length of honeycomb and two screens. The distance from the wind tunnel nozzle exit to the start of the exit diffuser is 754 mm. The diffuser has a variable throat area and was adjusted to yield a simple diverging flow area in these experiments. The wind tunnel used here was designed and built by Carroll[30] and then modified for the current research effort.

The wind tunnel test section provides optical access on all four sides of the test section through fused silica (top and bottom) and float glass (side) windows. The two side windows provide viewing areas 406 mm long by 36 mm wide. The top window provides a viewing area 330 mm long by 33 mm wide. The bottom window provides the same viewing area as the top except for the area blocked off by the 17.5 mm diameter counterbore in which the transverse jet nozzle is inserted. The jet nozzle has been inserted directly into the counterbore in the bottom window in order to maximize optical access.

During the experiments, the wind tunnel is run at a stagnation pressure of 241 kPa and a stagnation temperature of 295 K. A sonic, underexpanded, transverse jet with a 4 mm diameter is injected into the test section through the bottom window. The jet conditions for the current study are the following: P_{oj} = 476 kPa, T_{oj} = 295 K, and J = 1.7. These jet conditions provide a suitable jet penetration distance while achieving a sizable flowfield region around the jet orifice which is undisturbed by reflections of the bow shock from the top wall. The air for the jet is provided by a separate, regulated line running from the facility air supply to the jet nozzle. An Omega type K thermocouple is used to measure the gas line temperature and a 0-1.8 MPa Setra pressure sensor measures the line pressure.

As mentioned above, the exit diameter of the axisymmetric jet nozzle is 4 mm. The contour of the nozzle consists of a one quarter segment of a 3:5 (minor axis : major axis) ellipse such that the major axis of the elliptical segment is perpendicular to the jet nozzle flow direction. The thickness of the boundary-layer along the entire length of the test section wall has been measured during previous research by Carroll[30]. The jet nozzle was placed at a location where the boundary-layer thickness is of the order of the jet diameter. This location is 168 mm downstream of the leading edge of the wind tunnel's side window viewing area.

Diagnostic Techniques

This study employs schlieren and shadowgraph photography and a two-component, coincident LDV system. This section briefly describes these two diagnostic techniques.

Schlieren and shadowgraph photography are performed using a Xenon Corp. Model 437 Nanopulser with a pulse duration of about 25 ns. The linearly configured schlieren/shadowgraph system is set up and focused onto Kodak 3200 TMAX film in a Nikon F2 camera body equipped with a Micro-Nikkor 200 mm micro-lens.

The two-component LDV system is shown in Fig. 2. The system consists of the following six main components: a 4 W, Cooper Lasersonics (Lexel) argon-ion laser, two-component LDV optics, a six-jet atomizer, a digital burst correlator, a Gateway 2000 486-33 personal computer, and a traverse table. These components are described below.

The argon-ion laser output peaks at the following two lines: blue (488 nm) and green (514.5 nm). These peak lines correspond to the two laser

beams used to measure two components of velocity using the LDV optics.

The LDV optics are a Model 9100-7 TSI Inc. four-beam, two-component system. The system employs a 350 mm focal length transmitting lens and 13 mm beam spacing. The system uses a forward scatter configuration with an off-axis collection angle of 35°. The blue and green fringes of the measurement volume (MV) are oriented at 90° with respect to one another. Also, the fringes are oriented at 45° with respect to the crossflow direction in order to minimize fringe bias throughout most of the flowfield. Finally, two Bragg cells provide frequency shifting at 40 MHz; this results in fringe velocities of 540 m/s and 570 m/s for the blue and green beams, respectively. The characteristics of the measurement volume (MV) and LDV system are summarized in Table 1.

The seeder is a TSI Inc. Model 9306 six-jet atomizer. The seeder is used to generate polydisperse silicone oil seed droplets. Bloomberg[31] measured the diameter distribution of the droplets from this seeder and reports a mean diameter of 0.8 μm. The seeder provides a mist composed of high pressure air and the silicone oil droplets. This mist is injected into the wind tunnel through a 1/4" OD stainless steel manifold tube inserted into the plenum chamber. The jet flow is seeded at a location that is about 100 jet line diameters upstream of the injection nozzle.

The LDV system uses a TSI Inc. Model IFA 750 digital burst correlator signal processor to measure the Doppler frequencies. This processor uses digital signal processing (DSP) and a double-clipped time delayed autocorrelation. The processor samples at 16 different rates, filters each of these data streams independently, and then automatically selects an optimal sampling rate. It uses the double clipped autocorrelation method to achieve an effective 1-bit digitization rate of 1 GHz. This digitization rate provides a 0.05% (percentage of reading) resolution in the measurement of the Doppler frequency[32].

As shown in Fig. 2, the velocity data are stored in RAM in a Gateway 2000 486-33 personal computer. This computer runs TSI Inc. "FIND" LDV data acquisition software. In addition, a Quick Basic post-process data reduction routine performs coordinate transformations and calculates mean velocities, turbulence intensities, Reynolds shear stresses, and higher-order turbulence moments. This routine corrects for velocity bias using the interarrival time weighting method.

A detailed description of the design of the LDV system traverse table is given by Goebel [33]. The table is used to automatically traverse the transmitting and receiving optics along both directions (x-y) of the midline, transverse plane. Two Aerotech linear positioners move the table in the vertical direction. A third Aerotech positioner traverses the table in the horizontal direction. The positioners are equipped with optical encoders for position feedback. The positioners provide an accuracy of ±25 μm per 25 mm of travel. A controller which provides the positioner control signal is given instructions via a serial port of the Gateway computer. These instructions are generated by a Quick Basic program which, in turn, communicates with the TSI FIND Software used to acquire velocity data from the LDV signal processor (see Fig. 2).

Finally, an error analysis including the uncertainties associated with fringe spacing determination, velocity biasing, fringe biasing, velocity gradient biasing, statistical uncertainty (finite ensemble size), and processor accuracy has been completed. The estimated uncertainty in the mean velocity measurements is 2% of U_C, where U_C is the velocity of the crossflow upstream of the leading bow shock. The estimated uncertainty in the rms velocity fluctuation is generally 3% of U_C. However, the uncertainty in the rms fluctuations may be as high as about 10% of U_C for a small region near the windward side of the barrel shock and near the wall where velocity gradient biasing contributes to most of the error. Note that these estimates of velocity measurement uncertainty do not include the effects of particle lag through strong shocks. However, this effect is discussed below.

Results and Discussion

Schlieren/Shadowgraph Flow Visualizations

Schlieren and shadowgraph flow visualizations have been performed as a qualitative study of the TJISF flowfield. These flow visualizations were performed using both pure air and pure helium as the jet injectant. Visualizations were also done at several different jet-to-crossflow momentum flux ratios, J, in order to choose jet conditions suitable for the current study. Figure 3 shows a shadowgraph of the air jet case chosen for these experiments. The flow is from left to right and the jet is injected through the bottom wall at the location shown. Note that there exist at least 7 jet diameters of undisturbed flow before the first bow shock reflection intersects the transverse jet flowfield.

Visible in the photo is the Mach disk of the underexpanded sonic jet flow. Also, large-scale turbulent structures can be seen in the shadowgraph photo, although the characteristics of such structures are difficult to discern because of the line-of-sight integrating nature of schlieren/shadowgraph photography. As in the previously discussed PLIF results of VanLerberghe et al.[22], superimposed

shadowgraph images taken at random times suggest that there is little or no bow shock movement even in the area near the top wall where the bow shock is reflected. This result concerning flow steadiness greatly simplifies LDV data acquisition in that there is no need for conditional sampling due to bow shock motion. However, as mentioned above, the images of VanLerberghe et al.[22] show that the barrel shock structure may be unsteady, particularly on the windward edge of the barrel shock. Conditional sampling of this region is not feasible and the velocity measurements taken here reflect a time-average of the velocities in this small region of unsteadiness.

LDV Measurements

Velocity measurements in the midline, transverse plane were obtained at over 2,200 spatial locations. A number of characteristics of this TJISF flowfield make it a unique and challenging flow in which to obtain accurate velocity data. First, the mean velocity vectors cover a range of angles of about 240° and the velocity magnitudes range from zero to nearly 600 m/s. In addition, the maximum velocity occurs at an unknown location and unknown flow angle. The velocity gradients also range from zero in the freestream to about 400 m/s/mm on the windward side of the emerging jet barrel shock. These high gradients require that thousands of spatial locations be considered in order to resolve the details of the flowfield. The precise locations of the bow shock and its reflection, the lambda shock, the barrel shock, and the Mach disk are all unknown a priori. Finally, because the flow is highly three-dimensional with the large gradients described above, spatial resolution (i.e., effective measurement volume size) and accurate measurement volume placement are both important issues.

Because of the complexities described above, the process of obtaining mean and turbulent velocity measurements involved several steps. First, the LDV measurement volume was carefully located to within about 0.05 mm in all three coordinate directions . Next, several LDV optical setups were used until it was determined that the maximum, instantaneous particle velocities in the direction normal to the measurement volume fringes did not exceed the system's maximum measurable velocity. This latter velocity is determined by the optical setup, the frequency range of the signal processor, and the direction of the particle motion. Data on several increasingly fine grids were also obtained in order to locate high gradient regions. Since a wide range setting of the signal processor input filters (10-100 MHz) resulted in poor resolution and unacceptably low data rates, bandpass filters of about 40 MHz width were used throughout the flowfield. Therefore, the large gradients and high turbulence intensity of the near-jet region required that the automated data acquisition system be paused between each spatial location in order to check the current velocity data histograms and update the input frequency filter settings of the signal processor. This process resulted in the use of about five different input filter settings per channel and in literally dozens of input filter setting combinations.

The four-beam, two component LDV setup was used to measure velocities as close as 0.75 mm from the jet wall. A two-beam, one component LDV setup was used to measure the x-component of velocity down to about 0.1 mm from the wall. Four thousand and ninety-six velocity realizations were obtained at each location to ensure statistical certainty. Although the small time scales in this flow do not allow for high burst density measurements, the LDV system achieved coincident data rates in excess of 20,000 velocity measurements per second in the freestream. This data rate facilitated the acquisition of velocity measurements at the large number of locations needed to adequately resolve the transverse jet flowfield structure.

Measurement Locations

Figure 4 shows the transverse, midline plane LDV measurement locations. The measurement plane is located at $z = 0$, with the coordinate system origin at the center of the 4 mm diameter jet orifice. This plane extends from the bottom wall to a height of five jet diameters above the wall and from five diameters upstream of the jet centerline to seven diameters downstream. The majority of the measurements were made in the high gradient near-jet region. This region includes the barrel jet structure and extends from the bottom wall to a height of two jet diameters and from two diameters upstream to two diameters downstream. The maximum spacing between velocity measurement locations in the inner-jet region was 0.25 mm in the vertical direction and 0.5 mm in the horizontal direction. The minimum spacing throughout the measurement plane was 0.25 mm in both the horizontal and vertical directions. Finally, note that the x-component, two-beam LDV measurements near the wall (at $y = 0.5$ mm and below) were obtained only at locations upstream of $x = -2.0$ mm and downstream of 2.0 mm (i.e., on either side of the jet).

Approach Flow Measurements

The streamwise velocity component of the approaching freestream boundary-layer was measured down to about $y = 0.1$ mm. Figure 5 is a plot of the

boundary-layer velocity profile obtained five jet diameters upstream of the jet orifice center (x = - 20 mm). The velocity measurements are shown together with a curve fit of the form given by Sun and Childs[34] for compressible, turbulent boundary-layers. The integral thicknesses shown in the figure were determined using the ideal gas equation of state and the assumptions of negligible transverse pressure gradient, adiabatic wall, and a recovery factor of 0.89 as suggested by Kays and Crawford.[35] The values for the shape factor, wake strength parameter, and skin friction coefficient are also shown. The freestream Mach number across the wind tunnel in the transverse direction was measured to be 1.59 ± 1% (U_C = 446 m/s).

Mean Velocity Measurements

The mean velocity vector field of the transverse, midline plane is shown in Fig. 6. The experimental velocity data were placed on a uniform grid for the vectors shown in this figure. This was achieved by linear interpolation in both the x and y directions between the unequally spaced data. This interpolation routine preserved experimental data values that coincide with the locations shown. The crossflow direction is again from left to right with the 4 mm diameter jet injected from the bottom and centered at x = 0 mm. In all succeeding figures (including all vector and contour plots), the coordinate system is centered on the 4 mm diameter jet as shown in Fig. 1. Figure 6 shows the main features of the TJISF flowfield. The uniform freestream flow approaches the jet from the left. The velocity vectors clearly define the barrel shock region of the emerging jet core which is terminated by the Mach disk. The obstruction caused by the supersonic jet core results in low velocity areas in the near-wall regions on the windward and leeward sides of the jet. The location of the bow shock at the height of y = 20.0 mm can also be found by scanning the top row of vectors for a sudden, although slight, increase in the flow angle. The bow shock crosses the y = 20.0 mm line at x = 2.0 mm. This agrees with the information gained from the shadowgraph image study described above.

Figure 7 shows a close-up of the mean velocity vector field in the inner jet region. Note that velocity data in this region were obtained at more than twice the number of velocity vector locations presented. This figure shows the large gradients in the regions between the inner jet core and the crossflow. It also clearly shows the low velocity regions on the windward and leeward sides of the jet. The flow approaching the jet from the left side is subsonic because it has just passed through the normal section of the leading bow shock. The flow velocities outside of the boundary-layer increase in the transverse direction because of the curvature of the bow shock (see Fig. 3). The approaching boundary-layer grows quickly as it nears the windward side of the jet. The region near the wall is much like the flowfield of a cylinder in crossflow. The main difference is that, in this case, there is interaction between the jet and crossflow fluids in this region of adverse pressure gradient. The incoming flow above about y = 2. 5 mm is turned up with the jet and forms a three-dimensional shear layer region between the jet and the crossflow. The incoming flow below about y = 2.5 mm is turned down toward the wall and there is a back flow region near the wall between about x = -2 and -6 mm. The flow approaching the jet stagnates near x = -2.5 mm and y = 2.5 mm. This stagnation point lies between two regions of widely different velocity gradients. These regions are discussed in the next section.

Everett et al.[36] conducted surface oil flow visualization and surface pressure measurements using pressure-sensitive paint in the same facility as that of the present study. Their study shows that there are two reverse flow regions upstream of the jet and one reverse flow region downstream. The two upstream recirculation regions probably correspond to two horseshoe-shaped vortices which wrap around the windward side of the jet. The present LDV measurements can adequately resolve only the recirculation region immediately upstream of the jet. The other recirculation region upstream of the jet (beneath the lambda shock) is too small and near the wall to be adequately resolved in the current study. The recirculation region downstream of the jet was also too near the wall to be adequately resolved. The center of the recirculation region immediately upstream of the jet is at about x = -5 mm and y = 0.5 mm. Figure 7 also shows the low velocity region on the leeward side of the jet, near the wall.

Next, note that for y-coordinate values of about 1 to 3 mm, the region of the velocity field downstream of the leeward edge of the barrel shock accelerates rapidly as it moves downstream. This effect is probably caused by crossflow fluid which has moved around the circumference of the barrel shock and impinges on itself on the midline plane. This is important because it shows that crossflow fluid can quickly enter the region between the jet fluid and the wall which may be an important mechanism for mixing.

The underexpanded jet flow is sonic at the orifice exit plane and accelerates to supersonic conditions in the vertical direction. The small

boundary-layer at the nozzle exit of the jet is seen in the bottom row of vectors just above the jet exit. As expected, the supersonic jet core flows vertically until it reaches a region where it is strongly influenced by the outer jet flow and is turned over as it accelerates toward the Mach disk. The maximum velocity immediately preceding the Mach disk is 589 m/s at about x = 5.0 mm and y = 5.5 mm. Assuming adiabatic flow in the inner jet core, this velocity corresponds to a maximum Mach number of 2.66, just before the Mach disk.

Although the flow deceleration through the Mach disk is clearly shown by the measurements in Fig. 7, particle lag effects through this strong normal shock result in an apparent deceleration region of about 1.5 mm length. Note, however, that much of the jet fluid does not pass through the Mach disk but rather emerges from the barrel shock structure through the weaker oblique shocks which define its boundaries. The transverse, midline plane cuts this annular, supersonic jet region in half and, in the velocity field shown, this three-dimensional region shows up as two regions of supersonic flow into which the subsonic flow of jet fluid which passed through the Mach disk is entrained. The jet fluid which passed through the Mach disk has little transverse momentum flux and is quickly turned downstream. This is shown in Fig. 7 by the small velocities downstream of the Mach disk (near x = 7 mm and y = 6 mm). The greatest jet penetration is achieved by the supersonic flow which emerges from the windward side of the barrel shock. It is mainly this part of the jet flow which forms the supersonic mixing layer regions at the top of the jet trajectory.

Figures 8-14 show contour plots of experimental measurements for the transverse, midline plane. The experimental data for all contours presented here were placed on a uniform grid by a linear interpolation kriging routine of Spyglass Transform software. This interpolation routine preserves experimental data values that coincide with the locations shown. The contour plot data were then smoothed to avoid fluctuations that result from the interpolation.

Figure 8 shows contours of the mean streamwise velocity (U) field. The contour values are in m/s. First, these contours show the deceleration of the incoming 446 m/s crossflow due to the leading bow shock. These contours also clearly show the deceleration of the boundary-layer in the region of the bow shock wave/boundary-layer interaction upstream of the jet. The crossflow boundary-layer begins to decelerate at about x = -12 mm. Next, the reverse flow upstream of the jet is shown clearly as the area inside the zero velocity contour near the wall and between about x = -2 and -6 mm. Also, the contours show the region of velocity defect downstream of the Mach disk. Finally, the strong horizontal acceleration of the flow downstream of the barrel shock (and near the wall) is shown.

Figure 9 presents contours of the mean transverse velocity (V) field. Unlike the U contour plot, the large transverse velocities in the region of the inner jet clearly outline the boundaries of the barrel shock. Here, the leading bow shock is shown by the increase of transverse velocity of the incoming flow. However, this only occurs in the oblique regions of the bow shock. The strong transverse velocity gradients in the horizontal direction are clearly shown on the windward and leeward edges of the barrel shock near the nozzle exit. These gradients are strongly positive and negative, respectively. The rapid deceleration of the jet flow which passes through the Mach disk is clearly seen. Also, note the regions of large transverse velocity just above and below the Mach disk. These regions coincide with jet fluid that has passed through the weak shocks which define the sides of the barrel shock.

Figure 10 shows contours of the mean Mach number field. Again, we see many of the features of Figs. 8 and 9, including the change in Mach number through the leading bow shock, the rapid deceleration of the flow as it approaches the jet, and the rapid acceleration downstream of the jet. The barrel shock region is clearly outlined here and the Mach disk location and orientation are clear. Note that supersonic flow regions of jet fluid which passed through the oblique sections of the barrel shock are shown to surround an island of subsonic flow immediately downstream of the Mach disk. Finally, note that the Mach number contours on the leeward side of the barrel shock are more closely spaced than those on the windward side. This may be due to the slight unsteadiness of the windward side of the barrel shock that was discussed above. However, even the windward side has closely spaced Mach number contours which suggests that the effects of this unsteadiness are small.

Turbulence Measurements

Figures 11 and 12 show contours of the streamwise and transverse turbulence intensity ($\langle u' \rangle / U_C$ and $\langle v' \rangle / U_C$) fields of the x-y midline plane, respectively. The fluctuating velocities have been non-dimensionalized by the incoming, freestream velocity, U_C = 446 m/s. These plots show similar trends. First, they show the amplification of turbulence intensity in the region of the shock wave/boundary-layer interaction upstream of the jet. Next, the high turbulence intensity regions in the shear layer between the inner jet region and the crossflow are clearly seen. Note that the velocity measurements taken here reflect a time-average

of the velocities in the regions of barrel shock unsteadiness. As mentioned above, however, this unsteadiness is probably confined to a small region on the windward side of the barrel shock. The inner jet itself, like the freestream, is predominantly inviscid and shows low turbulence intensities. The turbulence intensity of the incoming freestream grows rapidly as the jet is approached and reaches its highest values very near the jet. The streamwise turbulence intensity reaches a maximum of 0.29 in this region at x = -5.0 mm and y = 0.75 mm (in the recirculation region immediately upstream of the jet). The transverse turbulence intensity also reaches a maximum of 0.32 on the windward side of the jet at x = -1.5 mm and y = 4.25 mm. In both plots, two regions of high turbulence intensity are also seen which lie just above and below the Mach disk in the shear layers on the windward and leeward sides of the barrel shock. Immediately downstream of these regions, the turbulence intensity decreases slightly. However, the turbulence intensity again increases in the region downstream of about x = 13 mm. This effect is most prominent in the $\langle v' \rangle / U_C$ field. The reason for this decrease and subsequent increase in turbulence intensity is not clear. It could possibly be due to a three-dimensional effect in these turbulent mixing regions. Perhaps the interaction of the kidney-shaped, crossflow plane vortices and the crossflow fluid generates turbulence in this manner. Finally, note that after about three diameters downstream (x = 12 mm), the regions of high turbulence intensity are confined to transverse locations below about 3.5 diameters and they don't seem to be spreading quickly. This upper bound is indicative of how far the jet has penetrated (for this momentum flux ratio).

Figure 13 shows a plot of the streamwise to transverse turbulence intensity ratio ($\langle u' \rangle / \langle v' \rangle$) contours. This ratio is a measure of the normal stress anisotropy of the turbulence in the x-y plane. The highest measured anisotropy of 1.7 occurs at about x = -5 mm and y = 0.75 mm (i.e. in the region of recirculation upstream of the jet). The lowest anisotropy of 0.6 occurs at about x = -1.5 mm and y = 4.5 mm on the windward side of the barrel shock. These locations of the anisotropy extremes are nearly identical to the locations of highest $\langle u' \rangle / U_C$ and highest $\langle v' \rangle / U_C$, respectively.

Figure 14 shows a plot of the Reynolds shear stress contours. The Reynolds stress is non-dimensionalized here by the square of the incoming freestream velocity. Near the region of the stagnation point on the windward side of the barrel shock there are two regions of peak intensities of Reynolds shear stress and these two regions are of opposite sign. These regions of high shear stress also correspond to regions of high mean velocity gradients. Therefore, large production of turbulent kinetic energy is expected to occur. The largest positive dimensionless shear stress of 0.08 occurs at about x = -4 mm and y = 2 mm. The large magnitude, negative shear stress of -0.056 occurs at x = -2 mm and y = 5 mm. Again, this suggests that these two regions have widely different velocity gradients. It is difficult to theorize on the production mechanisms of the $\langle u'v' \rangle$ Reynolds shear stress in these regions because the production term in the Reynolds stress equation for this component includes terms which are unknown. In addition, the stagnation point discussed above is very near (if not within) the region of barrel shock unsteadiness. The contour plot also shows the large negative and positive values of the Reynolds shear stress in the shear layers on the windward and leeward sides of the barrel shock, respectively. These two regions of opposite shear stress exist throughout most of the jet trajectory (far downstream, the Reynolds shear stresses are all negative). The high gradients regions of Reynolds shear stress across the jet cross-section, however, are diffused as the flow develops downstream. These same trends are seen in the turbulence fields of jets injected into subsonic crossflows[13]. Finally, note that the region of high Reynolds shear stress caused by the interaction of the jet and crossflow affects only a small part of the cross section of the midline plane for x-locations downstream of about three jet diameters (x = 12 mm).

Summary and Conclusions

Transverse jet injection into a supersonic flow (TJISF) is a promising method of achieving the injection, mixing, and combustion of fuel in new supersonic combustion engines. Despite the numerous studies of this flowfield, there are significant gaps in the knowledge base. Most notable is the dearth of quantitative, non-intrusive measurements of the mean velocity and turbulence fields. Therefore, such measurements add to the fundamental understanding of the fluid dynamic mechanisms and mixing processes of this flow. The present investigation provides LDV measurements of the mean and turbulent velocity fields of a sonic, underexpanded transverse jet injected into a Mach 1.6 flow. The study uses a two-component, frequency pre-shifted LDV system together with an automatic traverse system in order to provide measurements in the transverse, midline plane. The following observations have been made in addition to the discussion presented in the previous section.

1) The observed recirculation region of the jet under study extends as far upstream as 1.5 jet diameters and crossflow fluid as high as 0.5 diameters from the wall upstream of the jet may be turned upstream. Because of this, it may be possible for jet fluid to exist anywhere within this upstream recirculation region and this region could serve as an ignition zone in a reacting flowfield.

2) The fluid immediately downstream of the leeward side of the barrel shock accelerates rapidly in an area of low transverse velocity gradient. This, together with the fact that the Reynolds stresses in this area are small, suggests that a stream of unmixed, crossflow fluid wraps round the circumference of the barrel shock and impinges on itself in the region under the jet. Because of fluid entrainment caused by horseshoe vortices, this may be an important mechanism for mixing. Therefore, a designer should carefully choose the spanwise separation of jets in order not to impede this effect. Also, this effect determines the strength of the jet's wake and may influence the spacing of injector holes in the streamwise direction.

3) The Mach number of the jet immediately preceding the Mach disk was measured to be 2.66. The strength of the Mach disk is important because the jet loses much of its momentum flux here and is quickly turned downstream.

4) The measured contours of Mach number suggest that the region of unsteadiness on the windward side of the barrel shock is small. This issue is important not only because it affects the accuracy of the determination of shock location and the accuracy of the turbulence intensity measurements, but also because a designer may wish to promote unsteadiness in order to enhance mixing.

5) The configuration of the velocity vectors inside the barrel shock show that the jet fluid is bent toward the freestream before it has fully expanded to its highest velocity. Because of this (and to avoid the machining of supersonic injector nozzles) it may be advantageous to counter sink the exit holes of transverse jets in order to allow the jets to fully expand to high velocity before being influenced by the crossflow stream. Presumably, this would improve penetration.

6) The high Reynolds shear stress in the shear layer regions of the flowfield suggest areas of highly correlated (large-scale) structures. These regions are expected to have rapid mixing and, consequently, act as ignition locations in a reacting flowfield.

Acknowledgments

The authors would like to acknowledge the support of the Rocketdyne Division of Rockwell International Inc. under contract number R24QBZ92803049 with Dr. Munir M. Sindir as monitor. In addition, the first author would like to acknowledge assistantship support from the University of Illinois SURGE and Alumni Teaching Fellow programs.

References

[1]Adamson, T. C., Jr. and Nicholls, J. A. (1958). "On the Structure of Jets from Highly Underexpanded Nozzles into Still Air." *Journal of the Aero/Space Sciences*, **261**: pp. 16-24.

[2]Schetz, J. A. and Billig, F. S. (1966). "Penetration of Gaseous Jets Injected into a Supersonic Stream." *J. Spacecraft*, 3(11): pp. 1658-1665.

[3]Billig, F. S., Orth, R. C. and Lasky, M. (1971). "A Unified Analysis of Gaseous Jet Penetration." *AIAA Journal*, **9**(6): pp. 1048-1058.

[4]Heister, S. D. and Karagozian, A. R. (1990). "Gaseous Jet in Supersonic Crossflow." *AIAA Journal*, **28**(5): pp. 819-827.

[5]McDonough, J. and Catton, I. (1989). "Calculation of a Lateral Jet in a Hypersonic Cross-Flow." AIAA 89-2549, AIAA/ASME/SAE/ASEE 25th Joint Propulsion Conference, Monterey, CA.

[6]Segal, C., Haj-Hariri, H. and McDaniel, J. C. (1992). "A Numerical Investigation of Hydrogen Combustion in a Mach 2 Airflow." AIAA 92-0341, 30th Aerospace Sciences Meeting & Exhibit, Reno, NV.

[7]Clark, S. W. and Chan, S. C. (1992). "Numerical Investigation of a Transverse Jet for Supersonic Aerodynamic Control." AIAA 92-0639, 30th Aerospace Sciences Meeting & Exhibit, Reno, NV.

[8]Aso, S., Tannou, M., Maekawa, S., Okuyama, S., Ando, Y., Yamane, Y. and Fukuda, M. (1994). "A Study on Mixing Phenomena in Three-Dimensional Supersonic Flow with Circular Injection." AIAA 94-0707, 32nd Aerospace Sciences Meeting & Exhibit, Reno, NV.

[9]Riggins, D. W. and McClinton, C. R. (1992). "A Computational Investigation of Mixing and Reacting Flows in Supersonic Combustors." AIAA 92-0626, 30th Aerospace Sciences Meeting & Exhibit, Reno, NV.

[10]Keffer, J. F. and Baines, W. D. (1963). "The Round Turbulent Jet in a Cross-wind." *Journal of Fluid Mechanics*, 15(4): pp. 481-497.

[11]Kamotani, Y. and Greber, I. (1972). "Experiments on a Turbulent Jet in a Cross Flow." *AIAA Journal*, 10(11): pp. 1425-1429.

[12]Chassaing, P., George, J., Claria, A. and Sananes, F. (1974). "Physical Characteristics of Subsonic Jets in a Cross-stream." *Journal of Fluid Mechanics*, 62(1): pp. 41-64.

[13]Andreopoulos, J. and Rodi, W. (1984). "Experimental Investigation of Jets in a Crossflow." *Journal of Fluid Mechanics*, 138: pp. 93-127.

[14]Zukoski, E. E. and Spaid, F. W. (1964). "Secondary Injection of Gases into a Supersonic Flow." *AIAA Journal*, 2(10): pp. 1689-1696.

[15]Schetz, J. A., Hawkins, P. F. and Lehman, H. (1967). "Structure of Highly Underexpanded Transverse Jets in a Supersonic Stream." *AIAA Journal*, 5(5): pp. 882-884.

[16]Schetz, J. A., Weinraub, R. A. and Mahaffey, R. E., Jr. (1968). "Supersonic Transverse Injection into a Supersonic Stream." *AIAA Journal*, 6(5): pp. 933-934.

[17]Cohen, L. C., Coulter, L. J. and Egan, W. J., Jr. (1971). "Penetration and Mixing of Multiple Gas Jets Subjected to a Cross Flow." *AIAA Journal*, 9(4): pp. 718-724.

[18]McDaniel, J. C. and Graves, J., Jr. (1988). "Laser-Induced-Fluorescence Visualization of Transverse Gaseous Injection in a Nonreacting Supersonic Combustor." *J. Propulsion*, 4(6): pp. 591-597.

[19]Abbitt, J. D., III, Hartfield, R. J. and McDaniel, J. C. (1989). "Mole Fraction Imaging of Transverse Injection in a Ducted Supersonic Flow." AIAA-89-2550, AIAA/ASME/SAE/ASEE 25th Joint Propulsion Conference, Monterey, CA.

[20]Hermanson, J. C. and Winter, M. (1991). "Imaging of a Transverse, Sonic Jet in Supersonic Flow." AIAA-91-2269, AIAA/SAE/ASME 27th Joint Propulsion Conference, Sacramento, CA.

[21]Lee, M. P., McMillin, B. K., Palmer, J. L. and Hanson, R. K. (1991). "Two-Dimensional Imaging of Combustion Phenomena in a Shock Tube Using Planar Laser-Induced Fluorescence." AIAA-91-0460, 29th Aerospace Sciences Meeting, Reno, Nevada.

[22]VanLerberghe, W. M., Dutton, J. C., Lucht, R. P. and Yuen, L. S. (1994). "Penetration and Mixing Studies of a Sonic Transverse Jet Injected into a Mach 1.6 Crossflow." AIAA-94-2246, AIAA 25th Fluid Dynamics Conference, Colorado Springs, Colorado.

[23]Papamoschou, D., Hubbard, D. G. and Lin, M. (1991). "Observations of Supersonic Transverse Jets." AIAA-91-1723, AIAA 22nd Fluid Dynamics, Plasma Dynamics & Laser Conference, Honolulu, Hawaii.

[24]Fletcher, D. G. and McDaniel, J. C. (1989). "Laser-Induced Iodine Fluorescence Technique for Quantitative Measurement in a Nonreacting Supersonic Combustor." *AIAA Journal*, 27(5): pp. 575-580.

[25]Hartfield, J. R., Jr., Hollo, S. D. and McDaniel, J. C. (1992). "A Unified Planar Measurement Technique For Compressible Flows Using Laser-Induced Iodine Fluorescence." AIAA 92-0141, 30th Aerospace Sciences Meeting & Exhibit, Reno, NV.

[26]Hollo, S. D., McDaniel, J. C. and Hartfield, R. J., Jr. (1992). "Characterization of Supersonic Mixing in a Nonreacting Mach 2 Combustor." AIAA-92-0093, 30th Aerospace Sciences Meeting & Exhibit, Reno, NV.

[27]McDaniel, J. C., Fletcher, D., Hartfield, R. J., Jr. and Hollo, S. D. (1991). "Staged Transverse Injection into Mach 2 Flow Behind a Rearward-Facing Step: A 3-D Compressible Test Case for Hypersonic Combustor Code Validation." AIAA-91-5071, AIAA Third International Aerospace Planes Conference, Orlando, FL.

[28]Eklund, D. R., Fletcher, D. G., Hartfield, R. J., Jr., McDaniel, J. C., Northam, G. B., Dancey, C. L. and Wang, J. A. (1994). "Computational/Experimental Investigation of Staged Injection into a Mach 2 Flow." *AIAA Journal*, 32(5): pp. 907-916.

[29]Gallard, R., Geffroy, P., Jacquin, L. and Losfeld, G. (1993). "Etude Experimentale Sur Les Interactions Entre Un Jet Supersonique Chauffe Transversal Et Un Ecoulement Supersonique Externe." AGARD Computational and Experimental Assessment of Jets in Crossflow, Winchester, United Kingdom.

[30]Carroll, B. F. (1988). "A Numerical and Experimental Investigation of Multiple Shock Wave/Turbulent Boundary Layer Interactions in a Rectangular Duct." Ph.D. Thesis, University of Illinois at Urbana-Champaign.

[31]Bloomberg, J. E. (1989). "An Investigation of Particle Dynamics Effects Related to LDV Measurements in Compressible Flows." M.S. Thesis, University of Illinois at Urbana-Champaign.

[32]Jenson, L. (1991). "Automatic Digital Signal Processing For LDV." *ASME: Laser Anemometry*, **2**: pp. 617-628.

[33]Goebel, S. G. (1990). "An Experimental Investigation of Compressible, Turbulent Mixing Layers." Ph.D. Thesis, University of Illinois at Urbana-Champaign.

[34]Sun, C. C., and Childs, M. E. (1973). "A Modified Wall Wake Velocity Profile for Turbulent Compressible Boundary Layers." *Journal of Aircraft*, **10**(6): pp. 381-383.

[35]Kays, W.M., and Crawford, M.E. (1980). "The Turbulent Boundary Layer for a Gas with Variable Properties," *Convective Heat and Mass Transfer*, 2nd ed., McGraw-Hill, New York, pp. 305-309.

[36]Everett, D.E., Dutton, J.C., and Morris, M.J. (1995). "Pressure-Sensitive Paint Measurements of the Pressure Field About a Sonic Jet Injected Transversely Into a Mach 1.6 Freestream." AIAA 95-0524, 33rd Aerospace Sciences Meeting & Exhibit, Reno, NV.

Table 1: LDV system characteristics

Laser	4 W Cooper Lasersonics (Lexel) argon-ion laser
Beam lines	blue (488 nm)
	green (514.5 nm)
Bragg cell frequency shift	40 MHz
Beam expansion ratio	1.0
Transmitting lens	350 mm focal length
Beam Spacing	13 mm
Fringe Spacing	13.1 μm (blue)
	13.9 μm (green)
Fringe Velocity	540 m/s (blue)
	570 m/s (green)
No. of Fringes	12 (blue)
	12 (green)
MV diameter	0.17 mm (blue)
	0.17 mm (green)
Effective MV length (35° off-axis collection)	0.4 mm (blue)
	0.4 mm (green)
Signal Processor	TSI Inc. IFA 750 digital burst correlator
Seed particles	0.8 μm mean diameter silicone oil droplets

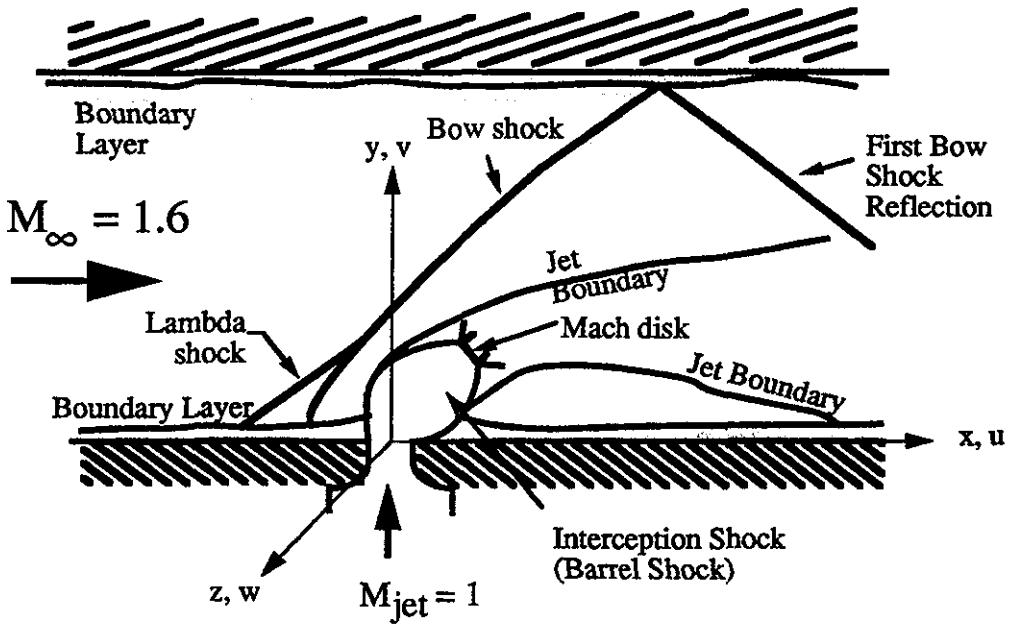

Figure 1: Typical flowfield of a sonic, underexpanded transverse jet injected into a supersonic flow

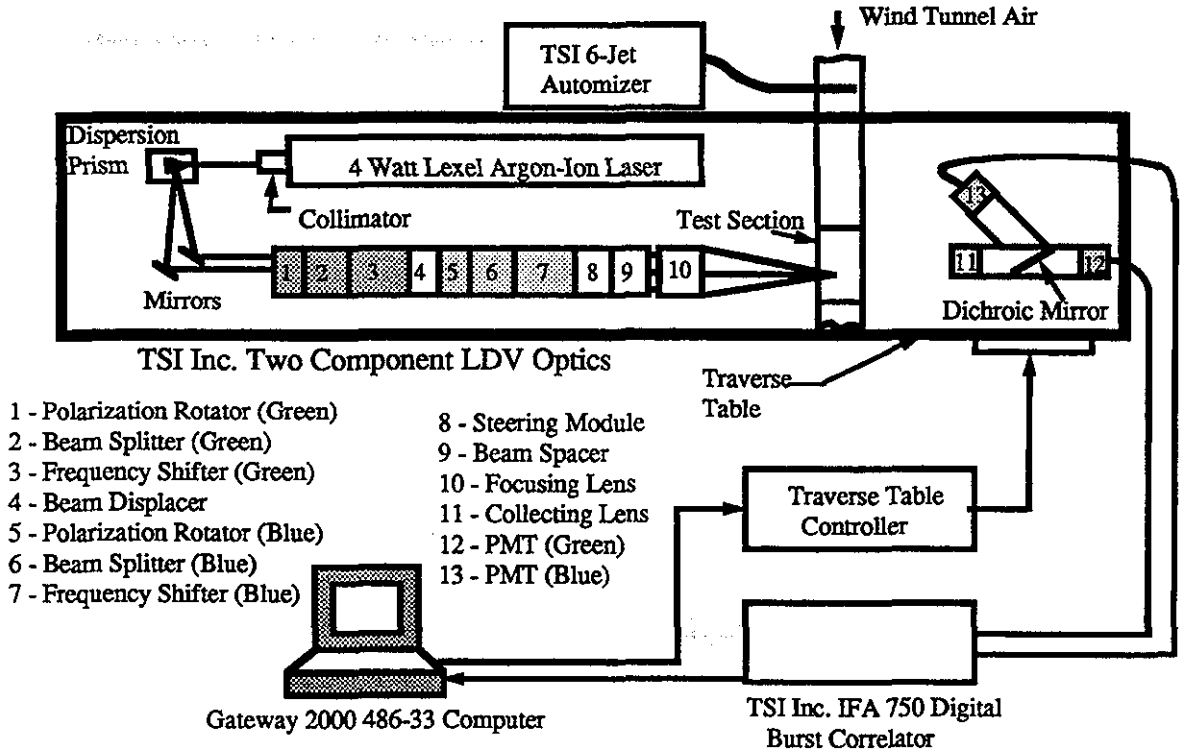

Figure 2: Two-component, frequency pre-shifted LDV system and automatic table traverse system

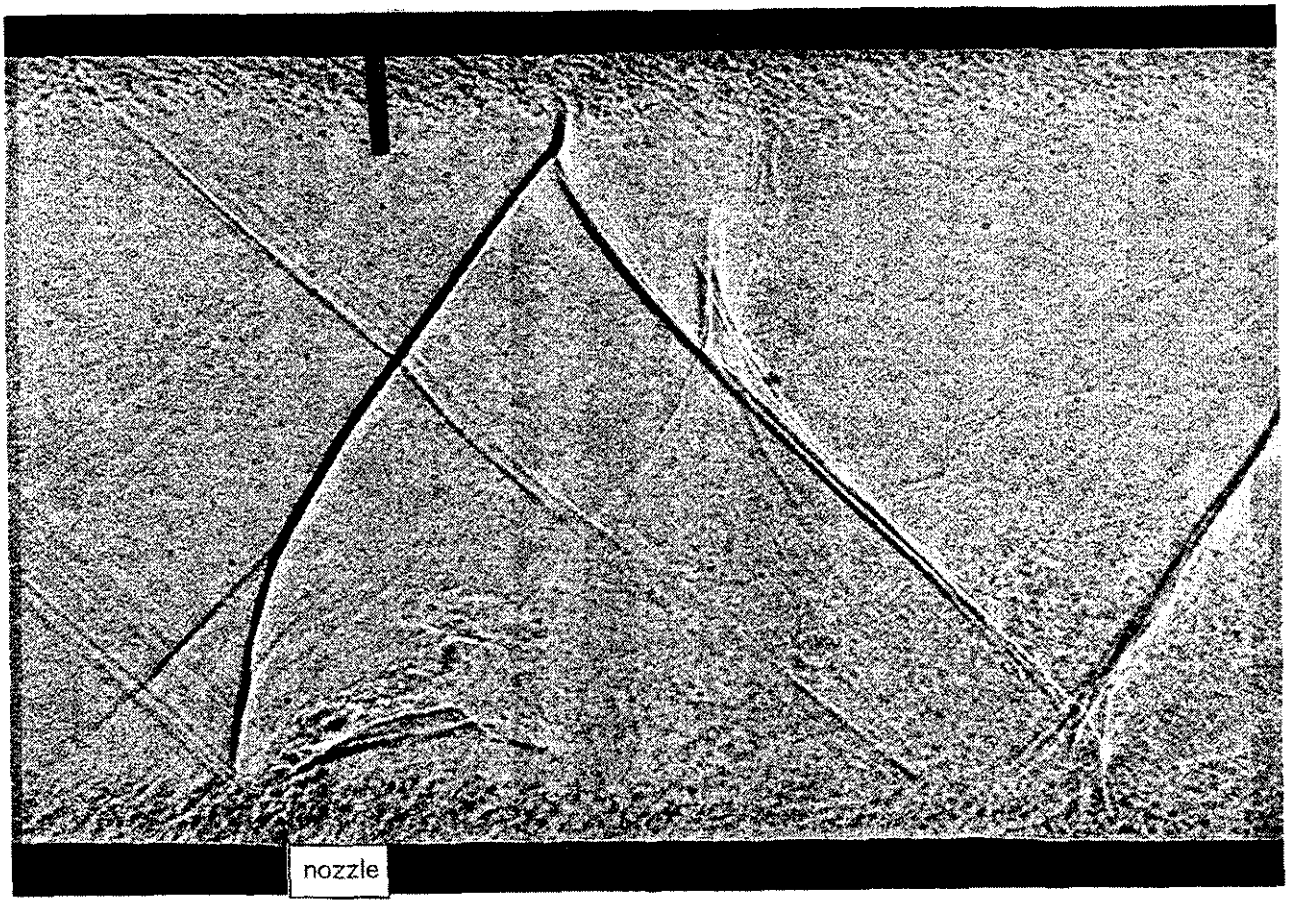

Figure 3: Shadowgraph of J = 1.7 air jet (flow is from left to right)

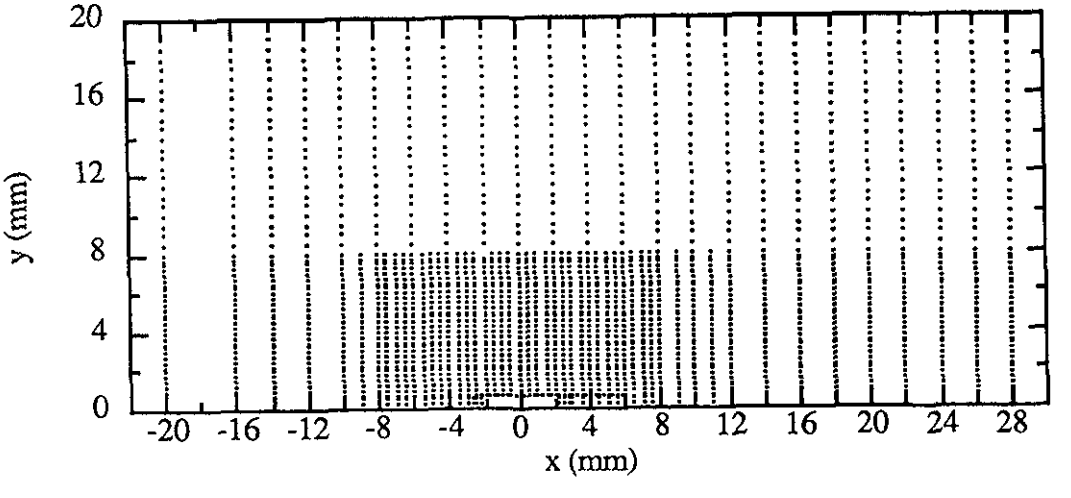

Figure 4: LDV measurement locations for midline transverse plane (jet centered at x = 0)

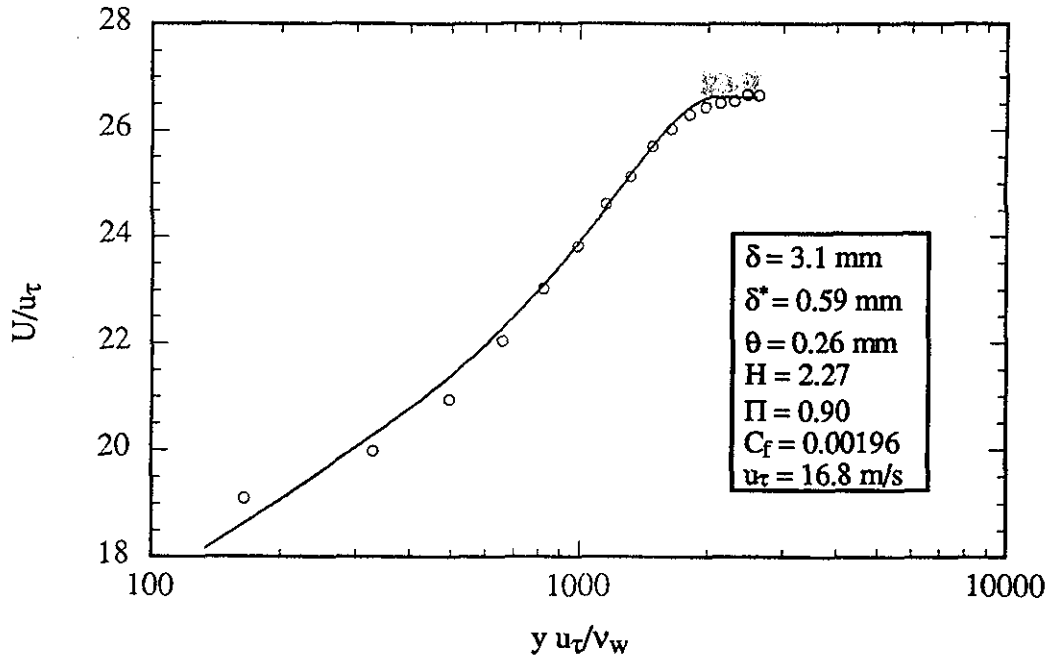

Figure 5: Sun and Childs[34] curve fit of approaching boundary-layer at x = -20.0 mm

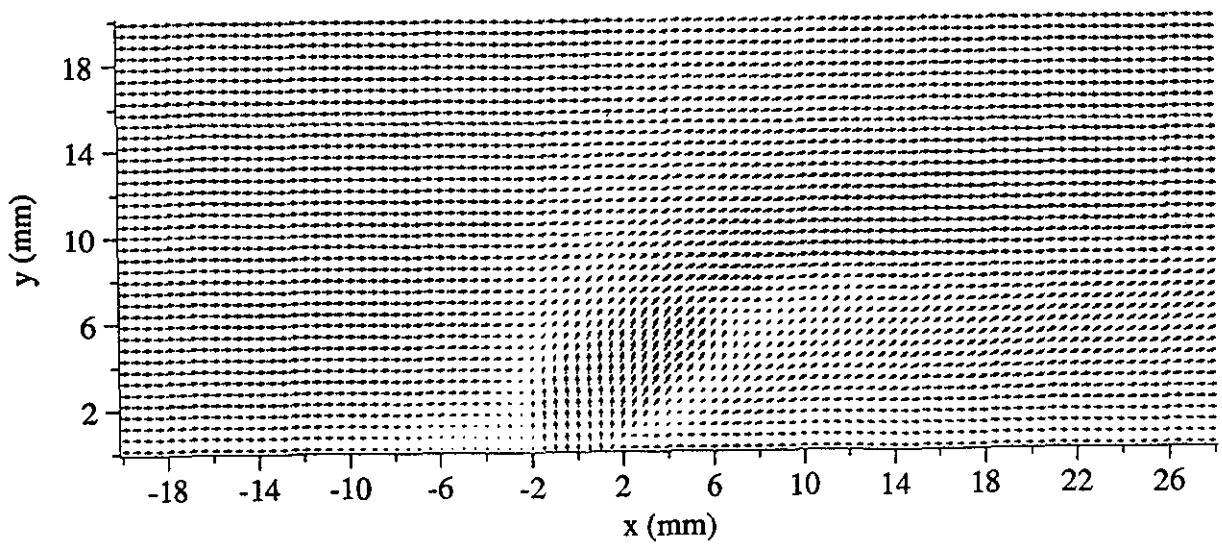

Figure 6: Mean velocity vector field of midline, transverse plane (jet centered at x = 0)

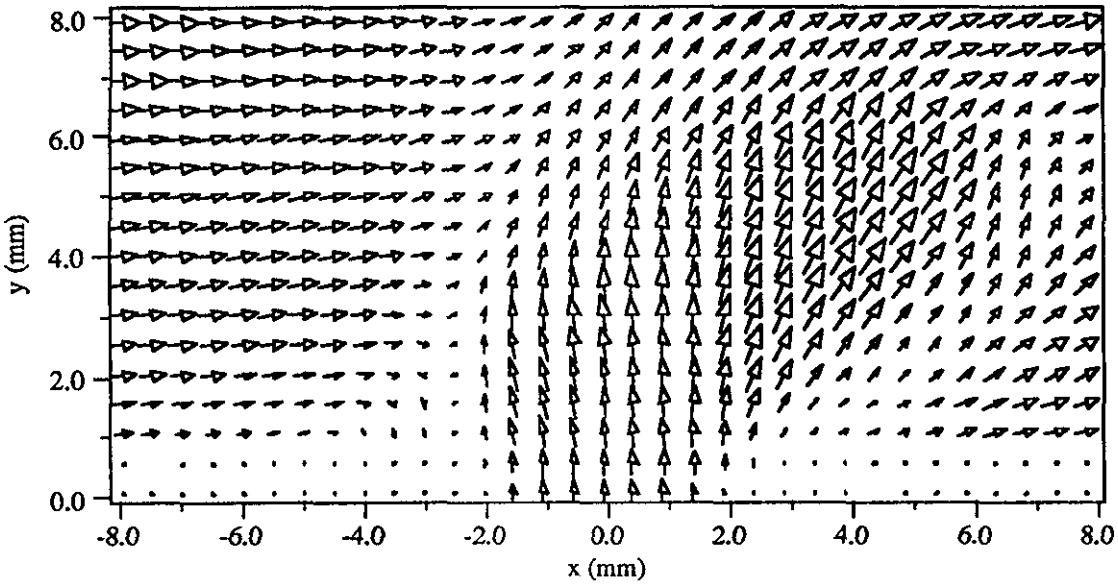

Figure 7: Mean velocity vector field of inner jet region (midline, transverse plane)

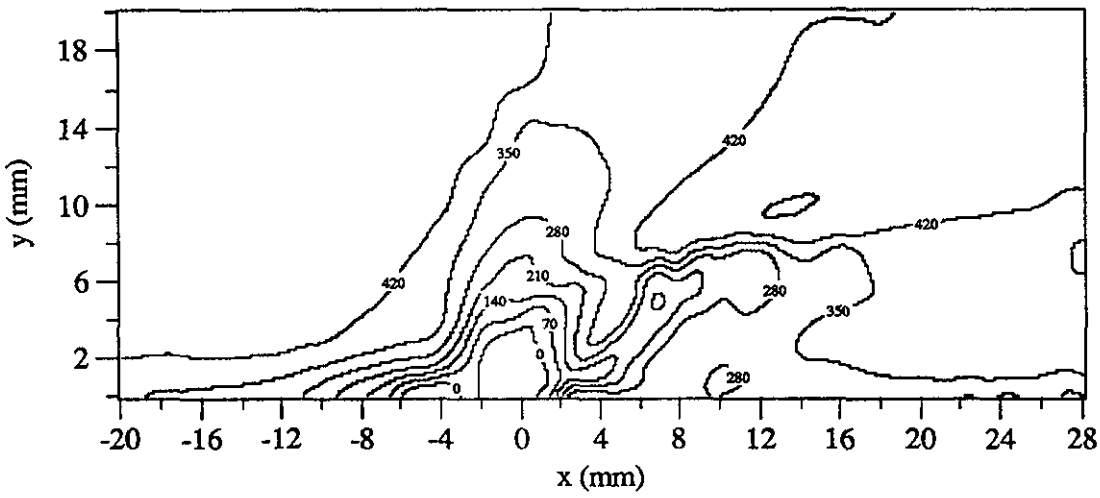

Figure 8: Mean streamwise velocity field of transverse, midline plane (velocity contours in m/s)

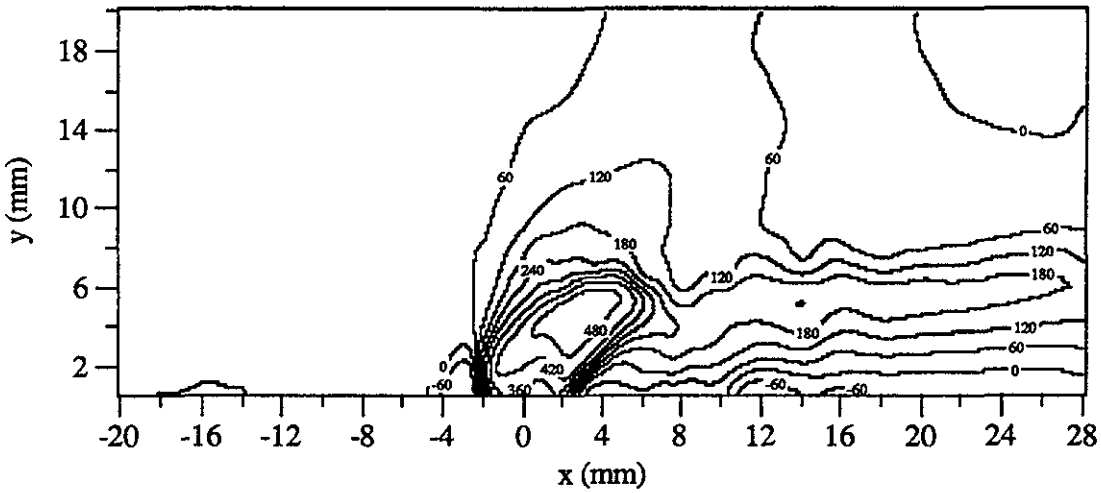

Figure 9: Mean transverse velocity field of transverse, midline plane (velocity contours in m/s)

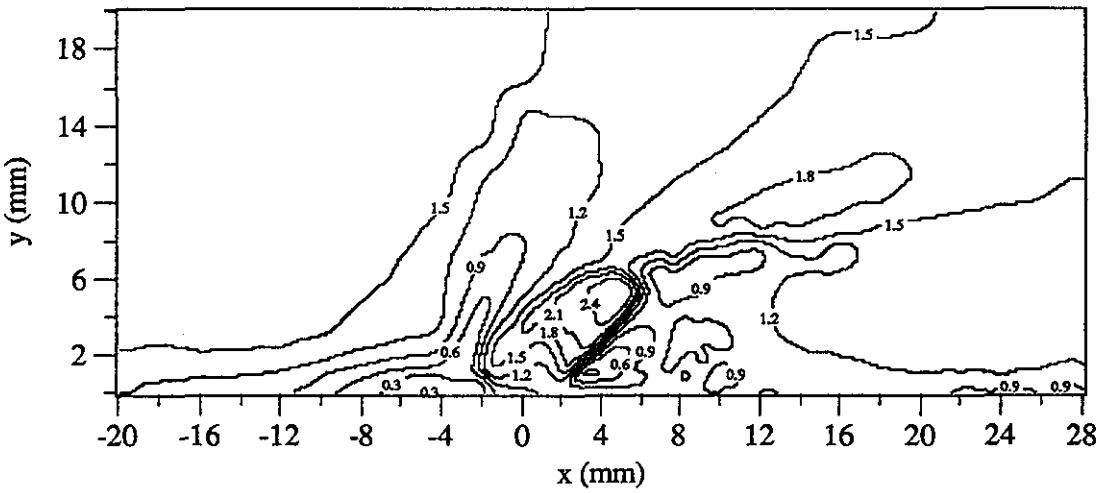

Figure 10: Mean Mach number field of transverse, midline plane

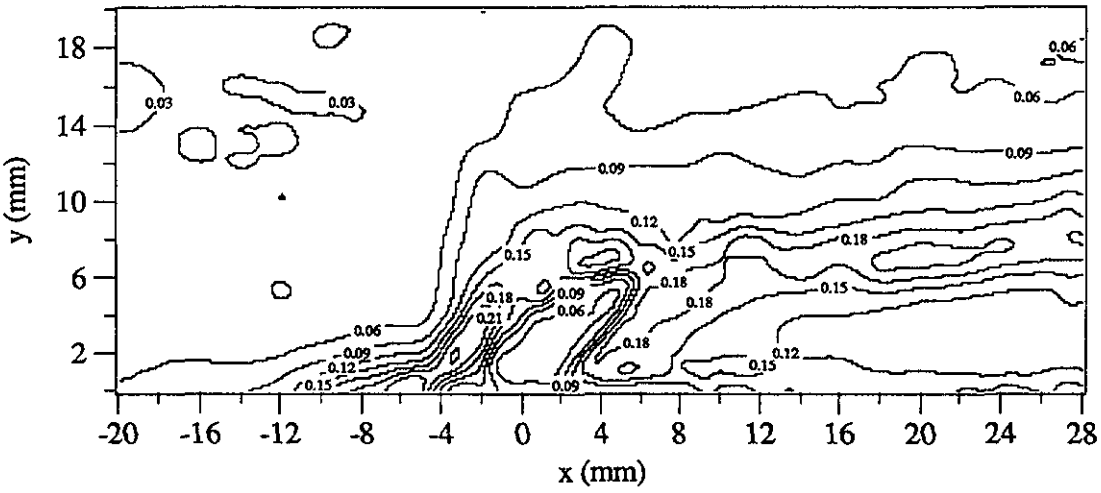

Figure 11: Streamwise turbulence intensity contours in transverse, midline plane ($\langle u' \rangle / U_c$)

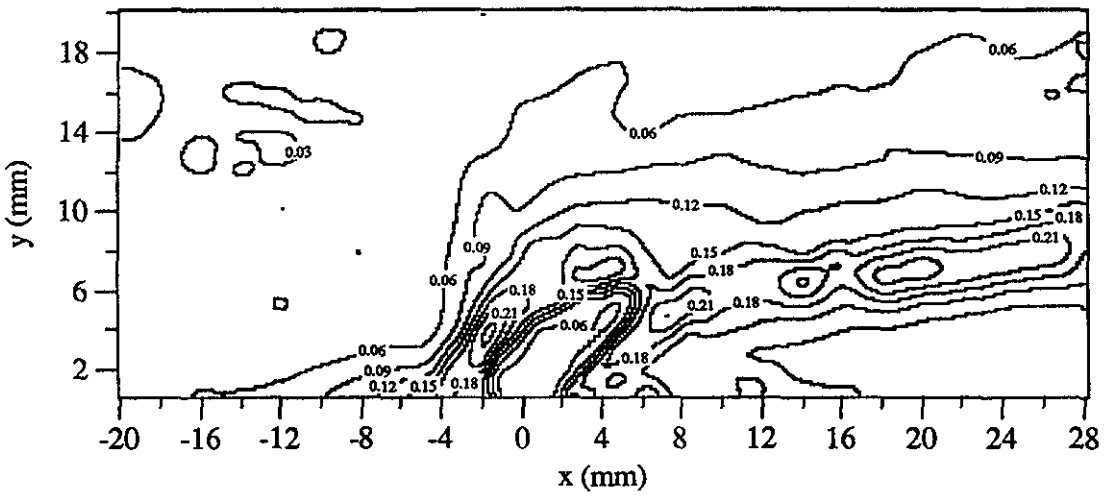

Figure 12: Transverse turbulence intensity contours in transverse, midline plane ($\langle v' \rangle / U_c$)

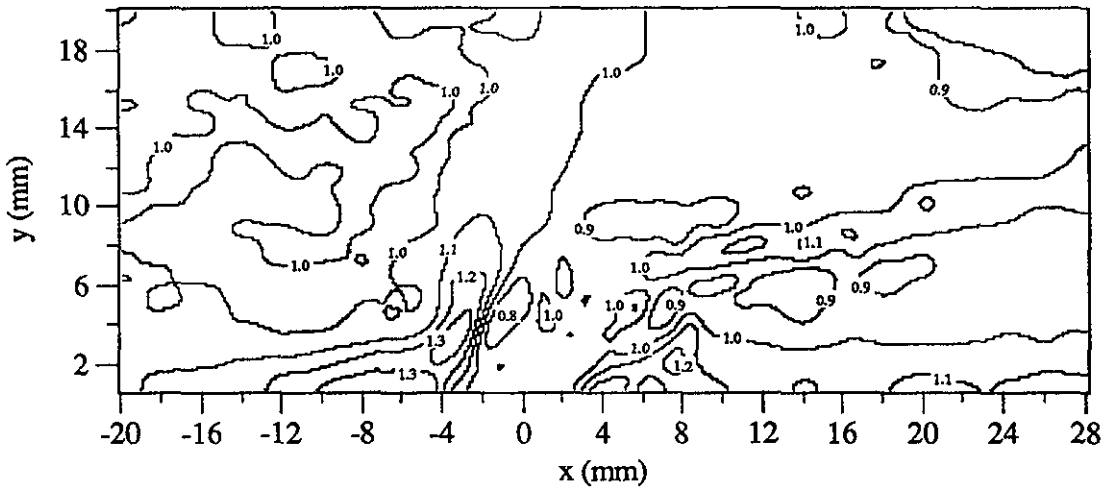

Figure 13: Streamwise to transverse turbulence intensity ratio contours in transverse, midline plane ($\langle u' \rangle / \langle v' \rangle$)

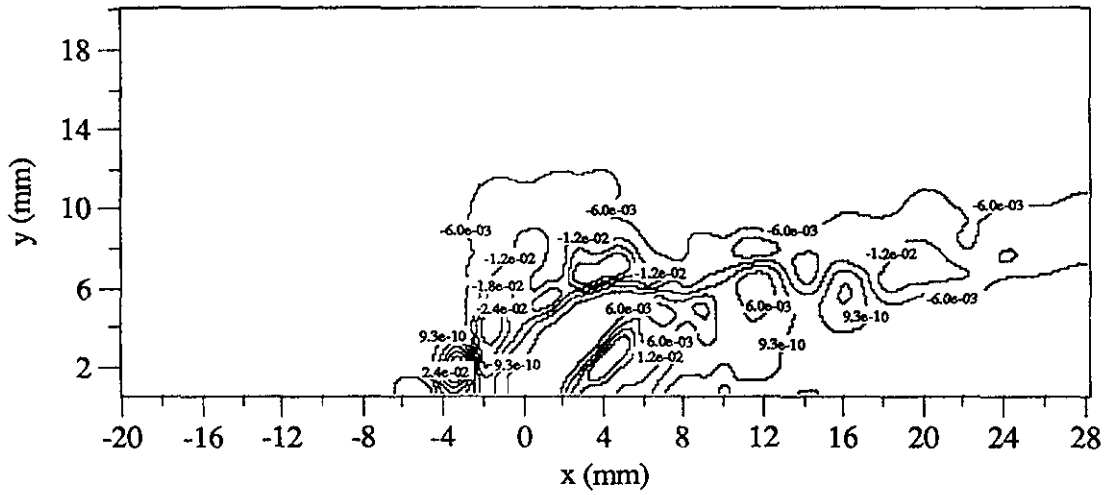

Figure 14: Reynolds shear stress contours in transverse, midline plane $\langle u'v' \rangle / U_c^2$